ELSEVIER

Thermochimica Acta 357–358 (2000) 285–291

thermochimica acta

www.elsevier.com/locate/tca

A calibration of the various heat-conduction paths for a heat-flux-type temperature-modulated DSC☆

I. Moon[a,b], R. Androsch[a,b], B. Wunderlich[a,b,*]

[a]*Department of Chemistry, The University of Tennessee, Knoxville, TN 37996-1600, USA*
[b]*Division of Analytical and Chemical Science, Oak Ridge National Laboratory, Oak Ridge, TN 37831-6197, USA*

Received 14 December 1998; accepted 15 March 1999

Abstract

A study was made of the effects of the heat-conducting paths from the temperature sensor to the sample and from the sample-temperature to the reference-temperature sensors on the determination of heat capacity in a temperature-modulated DSC (TMDSC) of the heat-flux type. These effects are usually assumed to be small. This is shown not to be so, and calibration procedures are developed. Using a simple model calculation, it is demonstrated that the phase angle difference between the sample temperature and the heat-flow rate should be taken into account when determining heat capacity. The results are experimentally verified for aluminum samples with various masses in quasi-isothermal experiments for a wide range of frequencies of temperature modulation for a Mettler–Toledo 820 DSC using no reference pan to simplify the analysis.

Keywords: Temperature-modulated DSC; Heat capacity; Phase angle; Calibration; Heat-flux DSC

1. Introduction

The temperature-modulated DSC (TMDSC) made a great impact on the ability to measure, identify, and separate the kinetics of various thermal responses and improved the understanding of the underlying mechanisms. It is the most important advantage of TMDSC to be able to separate reversible and irreversible latent-heat effects from the heat capacity, e.g. the hysteresis effect at the glass transition, the heat of chemical reaction, and the heat of fusion. Since the first description of the capabilities of the TMDSC method [1], there have been a number of efforts to determine the proper conditions for the measurement with TMDSC [2–12]. A more detailed investigation, however, is still needed to fully understand the thermal information derived from TMDSC experiments for the different types of calorimeters.

The basic analysis of TMDSC is derived from the well known alternating-current (ac) calorimetry [13]. The heat capacity C_s of a sample can be determined from the amplitude of the heat-flow rate response of the sample, represented by its amplitude A_{HF}, to the amplitude of the sinusoidal sample-temperature modulation, A_{T_s} and the modulation frequency ω ($=2\pi/p$, where p is the duration of the modulation period, usually given in seconds). The following equation gives the relationship for the case of ac

☆ Presented in part at the 26th NATAS Conference in Cleveland, OH, 13–15 September 1998. The submitted manuscript has been authored by a contractor of the US Government under the contract No. DE-AC05-96OR22464. Accordingly, the US Government retains a non-exclusive, royalty-free license to publish, or reproduce the published form of this contribution, or allow others to do so, for US Government purposes.

* Corresponding author.

0040-6031/00/$ – see front matter
PII: S0040-6031(00)00399-3

calorimetry:

$$C_s = \frac{A_{HF}}{A_{T_s}\omega} \quad (1)$$

In the case of TMDSC, additional factors should be considered because the twin calorimeters may not be identical in their environment [14]. The following equation was proposed for the reversing heat capacity from the heat-flux type TMDSC [2]:

$$(C_s - C_r) = \frac{KA_\Delta}{A_{T_s}\omega}\sqrt{1 + \left(\frac{C_r}{K}\right)^2\omega^2} \quad (2)$$

where C_r, K, and A_Δ are the heat capacity of the reference calorimeter (usually an empty aluminum pan), the Newton's law constant, assumed to describe the thermal conductance from the DSC heater to the sample and reference, and the amplitude of the temperature difference between the sample and reference temperatures ΔT ($=T_r - T_s$), respectively. For the derivation of Eq. (2), one had to assume that (1) there is no thermal conductance between the sample and reference calorimeters, (2) zero temperature gradients from the temperature sensors to the sample and the reference pans, and (3) also zero temperature gradients within the contents of the pans. In other words, one assumed infinite thermal conductance between temperature sensors and the corresponding calorimeters and their contents. It was, however, reported that, when using the heat-flux type DSC 2920 of TA instruments [5], the calibration factor which defines $(C_s - C_r)A_{T_s}\omega/A_\Delta$ depends not only on the frequency ω and the reference heat capacity C_r, as indicated by Eq. (2), but also on the sample mass. Furthermore, it is related to the phase-angle difference between the sample temperature and the heat-flow rate, which is influenced by the heat-transport conditions to and from the sample [6–8], and also by the thermal conductivity of the sample itself [9].

In this paper, we explore additional heat conducting paths inside the twin-calorimeter, as well as between the sample and the sensor as they may affect the determination of the reversing heat capacity in heat-flux type TMDSC. A simple model calculation is performed to obtain the format of the calibration function and information on the proper calibration conditions. The calculation results are tested with experimental data obtained from a Mettler–Toledo ADSC™ 820 calorimeter. A parallel analysis was made using a power compensation DDSC™ of Perkin–Elmer [15]. An experimental analysis using a TA Instruments MDSC™ which led to an assessment of the limits of applicability of Eq. (2) was presented earlier [16] and was used of the basis of a series of successful heat capacity determinations.

2. Experimental

A Mettler–Toledo 820 ADSC™ was programmed to have an amplitude of 0.5 K for both saw-tooth and sinusoidal modulations. Changing numbers of aluminum discs with a diameter of about 5.5 mm and a thickness of 0.14 mm were used as standard samples. The aluminum discs of a mass of about 9.0 mg each were placed in an open, standard aluminum pan of about 13.2 mg. Dry nitrogen was purged through the DSC cell with a flow rate of 20 ml min^{-1} and the cooling of the heat sink was accomplished with the liquid-nitrogen cooling accessory of the calorimeter. The sample temperature was initially calibrated in the standard DSC mode without temperature modulation, using the onsets of the transition peaks for indium and a series of additional secondary standards at a scanning rate of 10 K min^{-1}. All measurements were carried out in the quasi-isothermal mode at a T_0 of 298 K without use of a reference pan. Data were collected for 20 min, of which the last 10 min were used to obtain the first harmonic modulation amplitudes by Fourier-transform analysis after subtracting the zero baseline in the time domain (measured without sample and reference pans). In order to obtain a reference heat capacity of the aluminum used in these experiments, an amplitude calibration was made with a period above 150 s, calibrated with the known heat capacity of sapphire (22.14 mg), measured under the same condition as the aluminum.

3. Model analysis

Fig. 1 shows a schematic diagram of the Mettler–Toledo 820 ADSC™. In contrast to the heat-flux calorimeters of TA Instruments (MDSC™), which control the temperature modulation at the sample-sensor position, the ADSC™ is controlled at the block temperature T_b (furnace temperature output, see

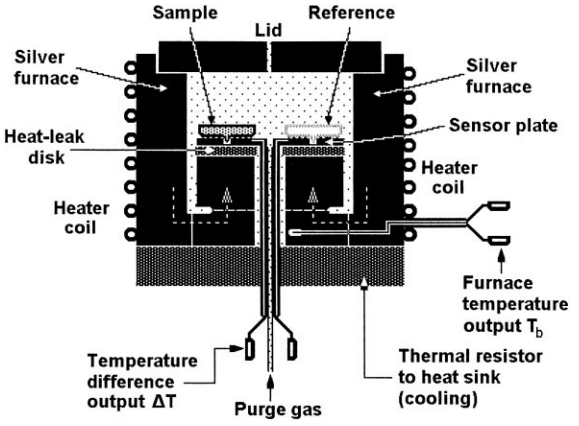

Fig. 1. Schematic diagram of the Mettler–Toledo 820 DSC.

Fig. 1). The difference between the two calorimeters lies in the response to changes in the heat capacity or apparent heat capacity to be measured. A change in the apparent heat capacity of the sample in an MDSC™ causes no change in the sample-temperature amplitude A_{T_s}, but increased heat-flux rate needed to keep A_{T_s} at the same value changes the reference-temperature amplitude A_{T_r}. In the ADSC™, the modulation of the block temperature is kept constant so that A_{T_r} does not vary, but A_{T_s} decreases with increasing apparent heat capacity of the sample calorimeter. The reference-temperature T_r of the ADSC™ is derived by calibration from the furnace temperature, T_b. The sinusoidally modulated temperature $T_b(t)$ is represented for the quasi-isothermal operation about the average temperature T_0 by the expression

$$T_b(t) = T_0 + A_{T_s} \sin\omega t \quad (3)$$

To analyze the thermal response of the Mettler–Toledo 820 calorimeter to the modulation of the heater, we set up the simple model of Fig. 2. For the present analysis, it is assumed that the furnace block has infinite thermal conductance. Also, sample and reference are assumed to contain no temperature gradients. The heat-conduction paths with finite thermal resistance are defined by (1) the heat-leak disk between the temperature-difference sensor and the furnace ($R=1/K$), (2) the path from sample to sample–thermocouple junctions, and (3) from reference to reference–thermocouple junctions (R_s, and R_r, respectively), and (4) the path between the thermocouple junctions at the sample and reference sides along the thermocouple wires and through the shared sensor plate (R', cross-flow). The heat conduction between the sample and the reference via the purging gas is neglected. Also neglected are the heat capacity effects of the thermocouple wires, the sensor plate, and the heat-leak disk, as well as the heat conduction from the sample and reference sides to the furnace block by the purge gas. In normal experiments, these effects are almost symmetrical for sample and reference sides and the temperature differences involved are small, so that they should lead to negligible effects.

There are analogies between the physical properties, temperature, heat-flow rate, heat capacity, thermal resistance and the electrical voltage, current, capacitance, and resistance, respectively. The analo-

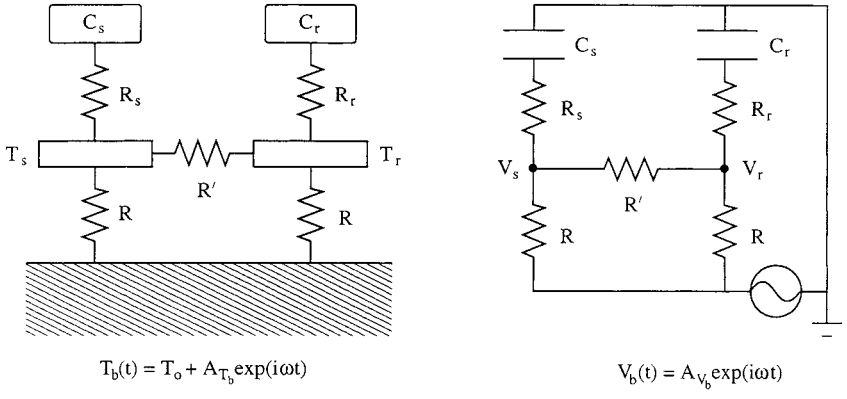

Fig. 2. Simple model for the TMDSC of Mettler–Toledo 820. The thermal resistances are R ($=1/K$), R', R_s and R_r, as explained in the text. The figure on the right illustrates the electrical-circuit analog which is the basis for Eq. (4).

gous network to the model calorimeter is shown on the right-hand side of Fig. 2 and can thus be used to calculate the temperature response of this model. On the basis of the well known electrical-circuit equation, the heat-capacity difference between sample and reference is given by

$$C_s - C_r = \left(\frac{2R+R'}{RR'}\right) \times \frac{A_\Delta}{A_{T_s}\omega} \frac{\sqrt{1+(\omega C_s R_s)^2}\sqrt{1+(\omega C_r)^2(R_r+(RR'/(2R+R')))^2}}{\sqrt{1+(\omega C_s C_r((R_s-R_r)/(C_s-C_r)))^2}} \quad (4)$$

Eq. (2) results from Eq. (4) with the assumptions R_s=R_r=0, R' is infinite, and K=1/R. The phase angle difference δ between T_s and ΔT (=T_r−T_s) can be written as

$$\delta = \phi_1 + \phi_2 + \phi_3 - \frac{\pi}{2} \quad (5)$$

and the three different phase components of δ can be seen from Eq. (4) to be

$$\phi_1 = \tan^{-1}(\omega C_s R_s) \quad (6)$$

$$\phi_2 = \tan^{-1}\left[\omega C_r\left(R_r + \frac{RR'}{2R+R'}\right)\right] \quad (7)$$

$$\phi_3 = \tan^{-1}\left(\omega C_s C_r \frac{R_s - R_r}{C_s - C_r}\right) \quad (8)$$

The three phase-lags of Eqs. (6)–(8) can then be used to simplify Eq. (4) to

$$C_s - C_r = \left(\frac{2R+R'}{RR'}\right)\frac{A_\Delta}{A_{T_s}\omega}\frac{\cos\phi_3}{\cos\phi_1\cos\phi_2} \quad (9)$$

Eq. (9) could be used for calibration to arrive at the corrected heat capacity using the phase information, but it is experimentally difficult to discriminate every phase term of δ, even though R_s can be set equal to R_r. If, however, one does not use a reference pan, i.e., C_r=0, then Eq. (9) reduces to

$$C_s - C_r = \left(\frac{2R+R'}{RR'}\right)\frac{A_\Delta}{A_{T_s}\omega}\frac{1}{\cos\phi_1} \quad (10)$$

where ϕ_1 can be directly determined from δ (=ϕ_1−(1/2)π). The same result can be derived from the model used in [6,7] if R' is assumed to be infinite and the heat capacity of the base plate is neglected.

For the case of the Mettler–Toledo 820 ADSC™, however, Eq. (10) can not be used directly for calibration because T_s is not measured by the temperature sensor. Its sensor plate with multiple thermocouple junctions at the sample and reference sides only yields ΔT. The measured sample temperature, T_s^m is determined from the calibrated reference temperature, T_r^*, and the temperature difference, ΔT, using $T_s^m = T_r^* - \Delta T$. For not too large modulation amplitudes, $T_r^*(t)$ can be linked to Eq. (3) with a simple calibration factor, which for simplicity of calculation was first set equal to 1.0. Experimentally, it could then be shown that this assumption is reasonable (see the results and the Fig. 4 given later in the text). With this assumption, T_s^m is given by

$$T_s^m(t) = T_0 + \frac{1+i\omega C_s(R_s+(R^2/(2R+R')))}{1+i\omega C_s(R_s+(R(R+R')/(2R+R')))}A_{T_b}\,e^{i\omega t} \quad (11)$$

which is not the same value as the actual sample temperature T_s. The measured heat capacity C_s^m is then related to the true sample heat capacity C_s through

$$C_s^m = \frac{K^* A_\Delta}{A_{T_s^m}\omega} = C_s\left(\frac{K^* RR'}{2R+R'}\right)\cos\left(\delta+\frac{\pi}{2}\right) \quad (12)$$

where K^* is the calibration factor, to be determined by a heat-flow-rate calibration. Using the heat of fusion of indium as a calibration experiment, K^* (=(2R+R')/(RR')) was found to be 30.5 mW K^{-1}. The value of δ is, furthermore

$$\delta = \phi_{T_s^m} - \phi_\Delta = \tan^{-1}\left[\omega C_s\left(R_s + \frac{R^2}{2R+R'}\right)\right] - \frac{\pi}{2} \quad (13)$$

Based on Eq. (12), one can now calibrate C_s^m for the Mettler–Toledo 820 ADSC™ for the conditions that were set for the derivation of the equation, i.e., for measurement without reference pans.

4. Results

In Fig. 3, the experimental data for C_s^m and δ are shown for a series of saw-tooth modulations with different periods and masses (open symbols). For the short periods p below 100 s (high frequencies ω),

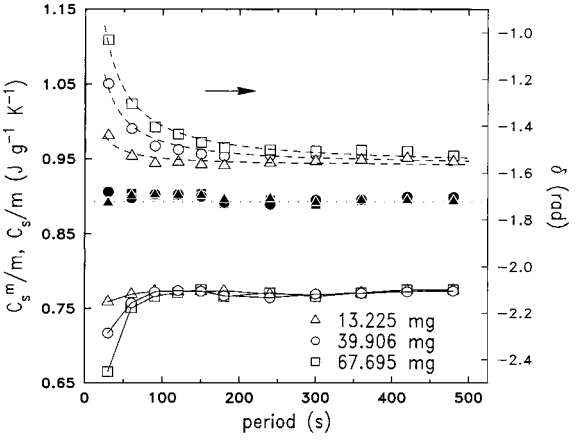

Fig. 3. The period and mass dependence of the measured specific heat capacity ($=C_s^m/m$) and the phase angle difference δ. The filled symbols represent the calibrated specific heat capacity C_s/m using Eq. (12). The dotted line denotes the specific heat capacity of Al, and the broken lines are the fitting results for δ, using Eq. (13) (right ordinate).

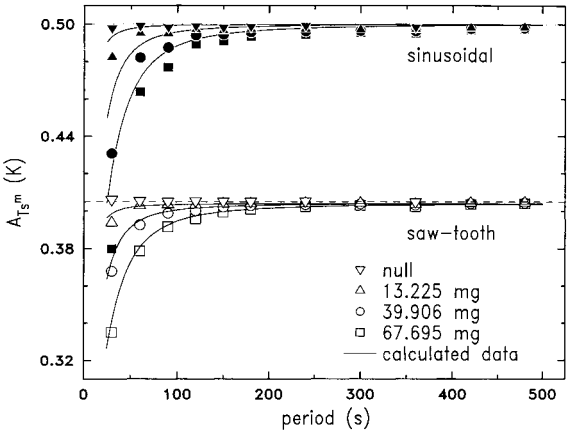

Fig. 4. The period and mass dependence of the first harmonic amplitudes of the measured sample temperatures, $A_{T_s}^m$. The dotted line at 0.5 K denotes the programmed amplitude and the dashed line represents the expected first harmonic amplitude for saw-tooth modulation. The open and filled symbols represent the measured saw-tooth and sinusoidal data, respectively. The solid lines are calculated from Eq. (11).

strong deviations occur from the known specific heat capacity of Al which is indicated by the dotted horizontal line. The constant negative offset from the measured heat capacity of Al over the whole range of periods was corrected by calibration with sapphire using Eq. (12) at large p where $\delta \approx -\pi/2$ (see upper part of Fig. 3 with the right ordinate). A value of 35.38 mW K^{-1} was found for K^* at 298 K.

The deviation at small p can be interpreted from Eq. (12) as originating from the coupling between the various thermal resistance parameters and C_s which is expressed by $\cos(\delta+(1/2)\pi)$. To determine the phase term, δ was fitted to Eq. (13) using calibrated heat capacity of aluminum (dotted line in Fig. 3). The fitting results of the measured δ are shown in Fig. 3 by the dashed lines. $R_s+R^2/(2R+R')$ of Eq. (13) has a value of $1.34/K^*$ which is independent of sample mass. Finally, the corrected heat capacity C_s was calculated with Eq. (12) from the measured C_s^m and δ values, and the $(2R\pm R')/RR'$ from the sapphire calibration. The results are shown in Fig. 3 by the filled symbols. All of the period and mass dependencies of C_s^m are removed by this calculation and correct heat capacities are obtained. The RMS error is 0.77%.

To confirm this calibration procedure, T_s^m was calculated by inserting the above values for $(2R+R')/RR'$ and $R_s+R^2/(2R+R')$ into Eq. (11). In Fig. 4, the calculated data (solid lines) show good agreement with the measured T_s^m for the saw-tooth modulation (open symbols). Note that the amplitude of the first harmonic, $A_{T_s}^m$, which represents the saw-tooth is, as expected, only 81% of the saw-tooth amplitude. The good agreement for the null measurement (zero baseline without sample and reference pans) proves that the temperature calibration factor for $T_r^*(t)$ is, indeed, close to 1, as assumed in Eq. (13).

A repetition of the same experiments with sinusoidal modulation results in Fig. 4 in the region of small p to large deviations between the calculated (solid lines) and measured data (filled symbols). Fig. 5 shows that C_s^m derived from the sinusoidal modulation (filled symbols) show also a very different period and mass dependence from the saw-tooth case (open symbols, same data as in Fig. 3). The calibration procedure developed for the saw-tooth modulation is, thus, in this case, not applicable to the sinusoidal modulation. A calibration using Eq. (12) would enhance the deviations rather than correct for the phase differences. The abnormal period and mass dependencies for the sinusoidal modulation can be attributed to the inability of the ADSC^{TM} used in this research to generate a perfect sinusoidal oscillation in the short-period range (below

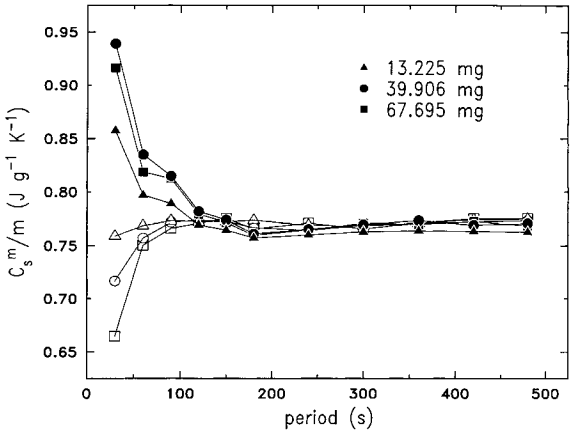

Fig. 5. The period and mass dependence of the measured specific heat capacity in the sinusoidal modulation (filled symbols) and the saw-tooth method (open symbols).

100 s). If the temperature controller operates linearly, the sinusoidal T_s^m and ΔT signals contain only first harmonic terms in the Fourier series describing their time dependence, while all odd harmonics are needed to perfectly fit T_s^m and ΔT in the saw-tooth method [10] (see also Fig. 4). However, the Fourier analysis of the sinusoidal ΔT shows for the ADSC^{TM} used in the present research a rather large ratio of the second harmonic amplitude to the first for small p. Fig. 6 reveals a 10% deviation for the case of a 30 s period.

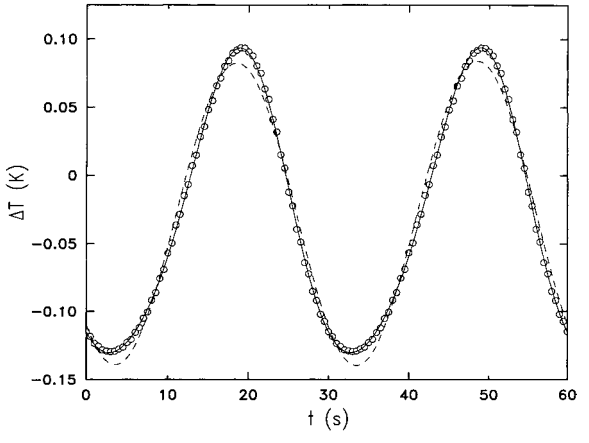

Fig. 6. The temperature difference ΔT as a function of time using sinusoidal temperature modulation (open circles). The broken line represents the first harmonic term of a Fourier fit. The solid line denotes the sum of the Fourier fit with a first and a second harmonic term (the ratio of the second harmonic amplitude to the first is about 0.1).

5. Discussion

For heat-capacity measurement of aluminum with a saw-tooth modulation using a Mettler–Toledo 820 ADSC^{TM}, calibration procedures for the period and mass dependence are given that lead to errors of less than 0.8% for periods down to 30 s. For periods of less than about 150 s, phase angle information needs to be generated to reach this precision. Therefore, it should be noticed that the usual sapphire calibration alone may not give correct heat capacities in the short-period region in TMDSC because correct calibration factors can be obtained only if there is no difference in the heat capacity values between the sapphire calibration and the chosen sample.

If the effect of thermal conductivity within the sample is negligible, this calibration procedure can also be used effectively in the phase-transition region where the apparent heat capacity of the sample is larger. A larger apparent heat capacity causes a larger phase-correction factor, even though the phase correction is not due to the small heat capacity value outside the transition region [11]. In the present case of aluminum, it was confirmed experimentally that there is no effect of the aluminum thermal conductivity since $R_s+R^2/(2R+R')$ shows no mass dependence; a sample of larger mass has lower thermal conductance in this experiment because the thickness of aluminum discs depends linearly on the mass.

In the TMDSC measurement with samples of low thermal conductivity as in the case of polymers, the thermal conductivity should be taken into account to obtain correct sample heat capacities. If there is a temperature gradient within the sample caused by low thermal conductivity, one can analyze this system approximately [12]. Since thermal resistance and heat capacity are additive quantities, one can consider serial coupling of the different thermal resistance values and parallel coupling of the different heat capacity values which are determined by a discrete sample-temperature distribution. Since, even in this case, the phase angle contains all of the relevant information, the same calibration procedure can be applied, even though some error is inevitable due to

the effect of the temperature gradient. To avoid complicated calibrations, it is therefore recommended to prepare thin samples with a large contact area to the sample pan in order to reduce the temperature gradient within the sample and the additional thermal resistance between the sample and the sensor. In case a reference pan is used and sinusoidal modulation is applied, it is shown in Figs. 4–6 that the measurements should be carried out in the period range where the amplitude of the sample-temperature oscillation has no deviation from the programmed amplitude.

Acknowledgements

This work was supported by the Div. of Materials Res., NSF, Polymers Program, Grant # DMIR-9703692 and the Div. of Materials Sci., Office of Basic Energy Sciences, DOE at Oak Ridge National Laboratory, managed for DOE by Lockheed Martin Energy Research Corp. (contract number DE-AC05-96OR22464). In addition, I. Moon expresses his appreciation of the Korea Research Foundation for support of his stay at the University of Tennessee.

References

[1] M. Reading, Trends Polym. Sci. 8 (1993) 248.
[2] B. Wunderlich, Y. Jin, A. Boller, Thermochim. Acta 238 (1994) 277.
[3] B. Wunderlich, A. Boiler, I. Okazaki, S. Kreitmeier, Thermochim. Acta 282/283 (1996) 143.
[4] B. Wunderlich, A. Boiler, I. Okazaki, K. Ishikiriyama, Thermochim. Acta 304/305 (1997) 125.
[5] S.R. Sauerbrunn, P.S. Gill, J.A. Foreman, in: Proc. 23rd NATAS Conf., 1994, p. 51.
[6] I. Hatta, S. Muramatsu, Jpn. J. Appl. Phys. 35 (1996) L858.
[7] I. Hatta, Thermochim. Acta 300 (1997) 7.
[8] T. Ozawa, K. Kanari, Thermochim. Acta 288 (1996) 39.
[9] J.E.K. Schawe, W. Winter, Thermochim. Acta 298 (1997) 9.
[10] B. Wunderlich, A. Boller, I. Okazaki, K. Ishikiriyama, W. Chen, M. Pyda, J. Pak, I. Moon, R. Androsch, Thermochim. Acta 330 (1999) 21.
[11] M. Merzlyakov, C. Schick, in: Proc. 5th Lähnwitz Seminar, Thermochim. Acta 330 (1999) 55, 65.
[12] B. Schenker, F. Stäger, Thermochim. Acta 304/305 (1997) 219.
[13] P.F. Sullivan, G. Seidel, Phys. Rev. 173 (1968) 679.
[14] B. Wunderlich, Thermal Analysis, Academic Press, Boston, 1990.
[15] R. Androsch, I. Moon, S. Kreitmeier, B. Wunderlich, Thermochim. Acta 357/358 (2000) 267–278.
[16] A. Boller, Y. Jin, B. Wunderlich, J. Therm. Anal. 42 (1994) 307.